

Collaborative Construction of a Silver Nanocluster Fluorescent Probe Using the Pyridinium-Based Ionic Liquid [C₄py][DCA]

Shu Wang, Enhui Zhou, Xuemei Wei, Ruanhui Liu, Changjiang Li, Le Pan, Yuchuan Zheng, and Nannan Xing*



Cite This: *ACS Omega* 2022, 7, 20241–20249



Read Online

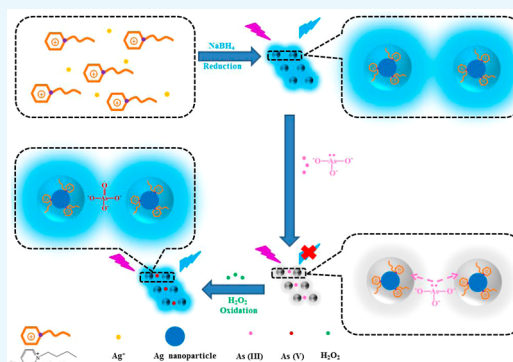
ACCESS |

Metrics & More

Article Recommendations

Supporting Information

ABSTRACT: A silver nanocluster fluorescent probe was synthesized by using the pyridinium-based ionic liquid [C₄py][DCA] as the protective agent, AgNO₃ as the precursor, and NaBH₄ as the reducing agent. The presence of pyridine group enhanced the fluorescence intensity of Ag nanoclusters and facilitated the coordination interaction between Ag nanoclusters and AsO₃³⁻. Therefore, the collaborative construction of a silver nanocluster probe using the pyridinium-based ionic liquid [C₄py][DCA] offered outstanding selectivity and sensitivity to detect AsO₃³⁻ in water. More interestingly, the fluorescent probe quenched by AsO₃³⁻ could be recovered with the addition of H₂O₂. This fluorescent probe provided a rapid and superior method for the detection of As(III) in the linear concentration range of 0–60 ppb with the lowest detection limit of 0.60 ppb. The mechanism of fluorescence quenching was a static quenching, considered to be due to electron migration between functional groups on the surface of Ag nanoclusters constructed with [C₄py][DCA] and AsO₃³⁻.



1. INTRODUCTION

According to the Survey of the World Health Organization, 80% of human diseases are related to water pollution.^{1,2} Trace elements in natural water are not only related to the geographical environment^{3,4} but also related to human activities such as the direct discharge of domestic wastewater, industrial wastes, and medical wastewater.⁵ Natural rock weathering and human exploitation and utilization of underground resources can bring arsenic into water sources, and the use of arsenic in chemical fertilizers and pesticides can also lead to trace arsenic in grains, vegetables, and water sources. Arsenic poisoning⁶ can occur if people drink water with high levels of arsenic for a long time. Therefore, the arsenic content is one of the important analysis indexes of water quality. Accurate determination of the arsenic content in water can not only guarantee the water safety of humans and livestock but also help to formulate effective treatment and protection measures according to water quality status and changing trends.^{7,8}

The toxicity of arsenic compounds is highly dependent on their form, and the toxicity of trivalent arsenic is much higher than that of pentavalent arsenic.⁹ Therefore, by finding only the total arsenic content in water quality monitoring, one cannot effectively estimate the harm of arsenic and correctly evaluate the environmental quality. It is more important for the selective determination of trivalent arsenic.^{10–12} At present, the main methods for the determination of arsenic contents are as follows: the colorimetric method with silver diethyl dithio-

carbamate,¹³ methylene blue,¹⁴ and other traditional colorimetric reagents, atomic absorption spectroscopy,¹⁵ inductively coupled plasma–mass spectrometry,¹⁶ high-performance liquid chromatography,¹⁷ and hydride generation atomic fluorescence spectrometry.^{18,19} The first analytical method is cumbersome, takes a long time, has low sensitivity and a narrow detection limit, and the organic solvent used in the analysis is harmful to the human body. Other methods overcome the above shortcomings and can be used to measure the total amount of arsenic. At the same time, the use of large instruments and equipment in the abovementioned traditional detection methods restricts the real-time, in situ detection.

Nowadays, various synthesis methods of metal nanoclusters have been proposed, and based on surface-enhanced Raman scattering (SERS), spectral absorption, and fluorescence optical properties of these metal nanoclusters, the sensors used for the detection of toxic and harmful ions in water have been widely used because of their advantages of being rapid, simple, and with high sensitivity. Boruah²⁰ et al. and Banerjee²¹ et al. detected As(III) in water using a colorimetric nanosensor with the LOD valued of 1 ppb and 0.86 ppb, respectively. Li²²

Received: April 7, 2022

Accepted: May 24, 2022

Published: June 2, 2022



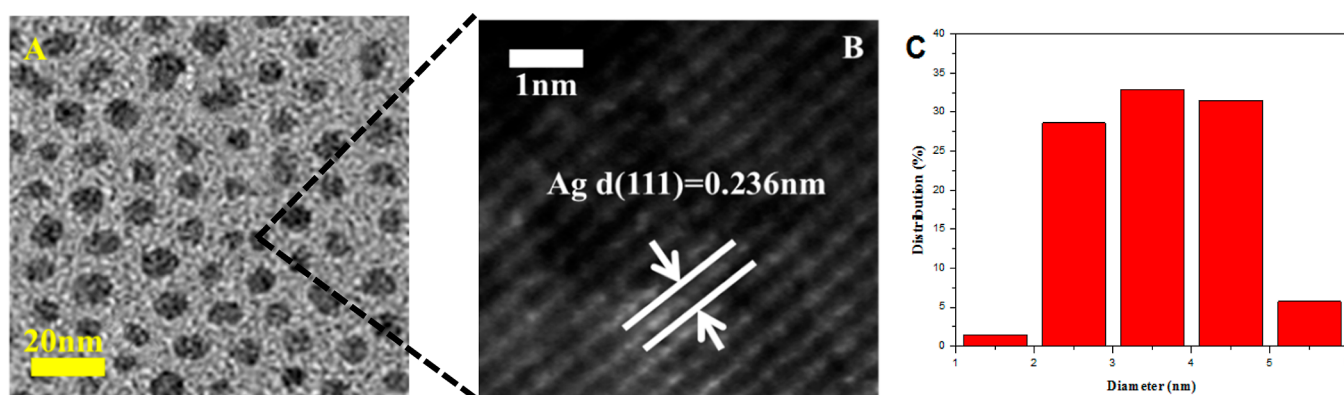


Figure 1. (A) TEM, (B) HRTEM, and (C) histogram of particle size distribution of AgNC-[C₄py][DCA].

et al. constructed a portable colorimetric and a fluorescence nanosensor with the LOD values of 0.87 and 0.66 ppb, respectively, to detect As(III) in water. Pathan²³ et al. and Sun²⁴ et al. found a fluorescence nanosensor with the LOD values of 5.1 and 1 ppb, respectively. Although the LODs of colorimetric and fluorescence nanosensors of As(III) in water have reached the standard LOD of 10 ppb recommended by WHO, nanosensors with a lower LOD are still required for its detection in actual water. Song²⁵ et al. developed a SERS nanosensor to detect As(III) in the linear concentration range of 0.5–10 ppb with a LOD of 0.1 ppb. Although the LOD had obviously improved, the narrow linear range of concentrations still restricted its application in actual water. Therefore, it is imperative to develop an optical sensor for As(III) detection in water with a low LOD and a wide linear concentration range.

Ionic liquids have been widely used in the field of physical chemistry because of their unique properties,^{26,27} such as non-combustion, very low vapor pressure, high thermal stability, a wide liquid range, a wide electrochemical window, and reusability. The excellent optical properties of ionic liquids containing metal elements have been recently reported, which indicated that it is feasible to construct metal nano-optical sensors by using ionic liquids.²⁸

In this paper, a kind of silver fluorescent probe coconstructed with an ionic liquid was prepared: [C₄py]-[DCA], a pyridine-based ionic liquid, and Ag nanoclusters were constructed in a cooperative construction mode. The positively charged silver nanoclusters were closely associated with AsO₃³⁻ by a coordination bond between the lone electron pair of AsO₃³⁻ and π molecular orbitals of the positively charged silver nanoclusters, and their original fluorescence can be quenched by the bond. More interestingly, AsO₃³⁻ was oxidized to AsO₄³⁻ with the addition of H₂O₂, and the original fluorescence gradually recovered with the disappearance of the lone electron pair of the anion.

2. EXPERIMENTAL SECTION

2.1. Reagents and Instruments. Table S1 in the Supporting Information shows the manufacturers and purity of all chemicals used. The synthesis of [C₄py][DCA] was based on the previous work of our research group, and the specific synthesis method was reported in the literature.^{28–31}

An ESCALAB 250 electron spectrometer with a monochromatic Al K α excitation ($h\nu = 1486.6$ eV) source was used for XPS measurements of materials. A JEOL-2010 high-resolution transmission electron microscope was used for transmission electron microscopy (TEM) experiments. The

fluorescence performance was measured using a F-4500 fluorescence spectrometer produced by Hitachi of Japan. A Shimadzu UV2000 UV–vis spectrometer was used to detect UV–vis spectra. A Nicolet380 Fourier transform infrared spectrometer was used to detect infrared spectra. A Malvern Zetasizer nano ZS90 nanoparticle size and potential detector was used to perform the dynamic light scattering (DLS) and apparent zeta potential experiments.

2.2. Preparation of Fluorescent Silver Nanoclusters.

In a typical synthesis of silver nanoclusters, 5 mL of triple distilled water and methanol with a volume ratio of 1:1 was added to the reaction bottle and mixed evenly; 5 mL of 2×10^{-2} mol·L⁻¹ AgNO₃ solution and 2 mL 5×10^{-2} mol·L⁻¹ [C₄py][DCA] were added to the above mixture system in turns dropwise; after 30 min, 5 mL of 1 mol·L⁻¹ NaOH solution was added dropwise into the above solution and was left to stand for 10 min; then, 0.5 mL of 0.1 mol·L⁻¹ NaBH₄ solution was added to the above mixture solution, which yielded silver nanoclusters after 3 h and was named AgNC-[C₄py][DCA]. The whole synthesis process was carried out in a thermostatic water bath, and the temperature was controlled at 40 °C.

2.3. Fluorescence Detection of AsO₃³⁻. The sensitive fluorescence detection of AgNC-[C₄py][DCA] to AsO₃³⁻ was as follows: 2 mL AgNC-[C₄py][DCA] solution was mixed with 2 mL different concentrations of AsO₃³⁻ from 10 to 600 μ g/L, and 16 mL triple distilled water was added to incubate for 5 min. The fluorescence of the solution was measured in 2 mL AgNC-[C₄py][DCA] solution mixed with 18 mL triple-distilled water as blank control.

The selective fluorescence detection of AgNC-[C₄py]-[DCA] to AsO₃³⁻ was as follows: 2 mL AgNC-[C₄py][DCA] solution was added to 18 mL 60 μ g/L AsO₃³⁻ and interfering ion solution, respectively, the interfering ions include cations (Na⁺, Mg²⁺, Al³⁺, Fe³⁺, Ag⁺, and Cu²⁺) and anions (CO₃²⁻, SO₄²⁻, NO₃⁻, PO₄³⁻, AsO₄³⁻, and PO₃³⁻), and the fluorescence detection conditions were the same as above.

The anti-interference ability detection of AgNC-[C₄py]-[DCA] to AsO₃³⁻ was as follows: 2 mL AgNC-[C₄py][DCA] solution was added to 18 mL mixed solution of 10 μ g/L AsO₃³⁻ and 60 μ g/L interfering ions, the interfering ions include cations (Na⁺, Mg²⁺, Al³⁺, Fe³⁺, Ag⁺, and Cu²⁺) and anions (CO₃²⁻, SO₄²⁻, NO₃⁻, PO₄³⁻, AsO₄³⁻, PO₃³⁻), and the fluorescence detection conditions were the same as above.

The recovery experiment of the fluorescence probe AgNC-[C₄py][DCA] was investigated by adding a certain concen-

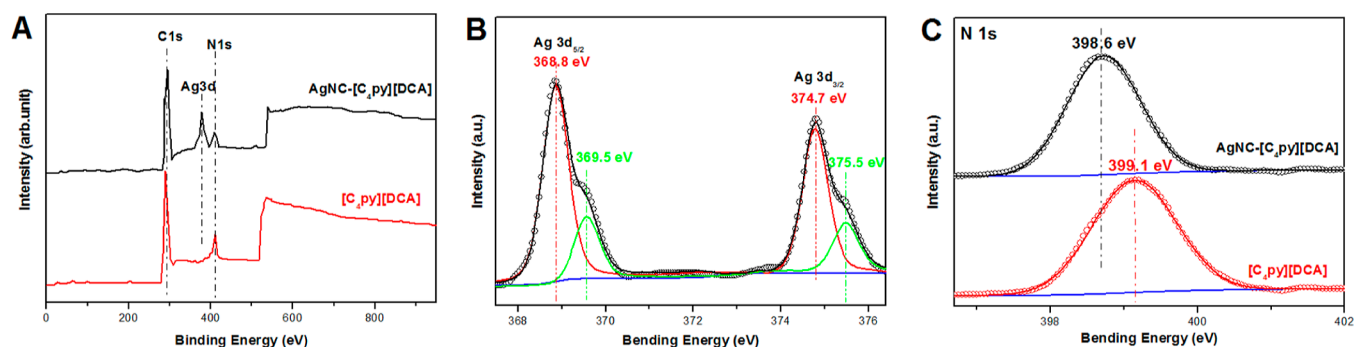


Figure 2. (A) Full scan X-ray photoelectron spectrum pattern and (C) N 1s high-resolution XPS patterns of AgNC-[C₄py][DCA] and [C₄py][DCA], (B) Ag 3d high-resolution XPS patterns of AgNC-[C₄py][DCA].

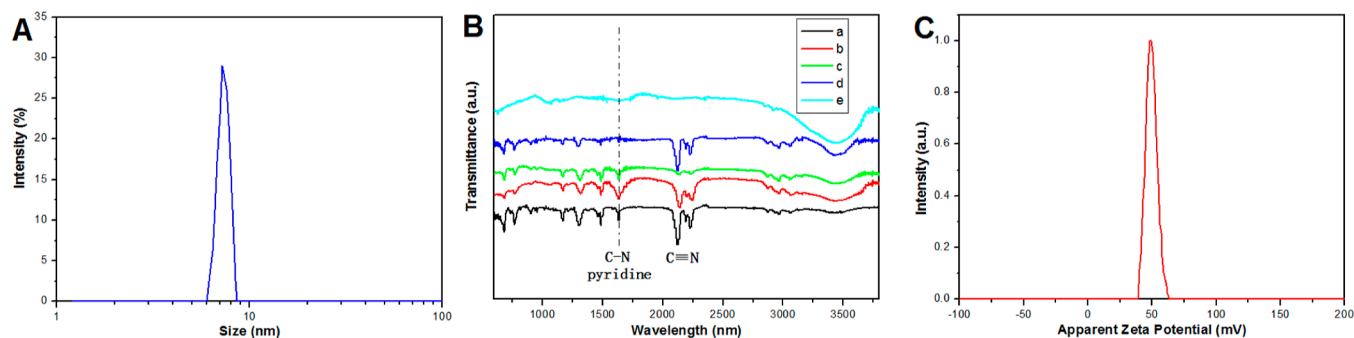


Figure 3. (A) DLS results of AgNC-[C₄py][DCA], (B) FTIR spectra of (a) [C₄py][DCA], (b) initial product of AgNC-[C₄py][DCA] after dialysis purification, (c) final product of AgNC-[C₄py][DCA] after repeated dialysis purification, (d) semipermeable extramembrane equilibrium solution of the initial product, and (e) semipermeable extramembrane equilibrium solution of the final product, and (C) apparent zeta potential of AgNC-[C₄py][DCA].

tration of hydrogen peroxide solution into the solution fluorescence quenched by AsO₃³⁻.

3. RESULTS AND DISCUSSION

3.1. Characterization of AgNC-[C₄py][DCA]. The size and morphology information of silver nanoclusters (AgNC-[C₄py][DCA]) constructed in collaboration was obtained by TEM and DLS experiments. The data in Figures 1A and 3A showed that the size of the silver nanoclusters was small and uniform. The ordered lattice fringes with a spacing of 0.236 nm in Figure 1B were observed for the (111) crystal plane of silver. The TEM particle size distribution statistical results (Figure 1C) and DLS average results (Figure 3A) showed that the size distribution of silver nanoclusters was uniform, and the average size was 4 nm and 7 nm, respectively.

The surface element composition and binding information of silver nanoclusters were detected by X-ray photoelectron spectroscopy and infrared spectroscopy. According to the full scan X-ray photoelectron spectral pattern of silver nanoclusters (AgNC-[C₄py][DCA]) and one of the raw materials for synthesis ([C₄py][DCA]) (Figure 2A), it can be seen that the N element in [C₄py][DCA] was successfully linked to the surface of silver nanoclusters. The Ag 3d_{3/2} XPS peak in Figure 2B could be effectively divided into two peaks corresponding to the binding energies³² at 368.8 and 369.5 eV, respectively. As can be seen from the binding energy data of the N 1s XPS peak of AgNC-[C₄py][DCA] and [C₄py][DCA] in Figure 2C, as [C₄py][DCA] formed AgNC-[C₄py][DCA], the binding energy of N 1s decreases from 399.1 to 398.6 eV, which means that the density of electron cloud around N atoms increased during this process.³³ Combined with the two splitting peaks of

Ag 3d_{3/2} in Figure 2B, the two species of Ag in the synthesized Ag nanoclusters can be classified as two silver species, one was the free Ag nanoparticles³⁴ with a binding energy 368.8 eV and the other was Ag nanoparticles with a binding energy of 369.5 eV bound to N atoms in [C₄py][DCA].

Figure 3B showed the infrared spectral data of various materials of the silver nanoclusters in the synthesis and purification process. As shown in the infrared spectrum of Figure 3B, the absorption peak at 3443 cm⁻¹ was attributed to the stretching vibration of the hydroxyl group (O–H). Because this peak was hardly visible in the infrared absorption spectrum of raw material [C₄py][DCA] and O element was not seen in the full XPS spectrum of AgNC-[C₄py][DCA], the infrared absorption peak at 3443 cm⁻¹ of each substance in Figure 3B was attributed to the stretching vibration peak of the hydroxyl group (O–H) in water and the surface hydroxyl group (O–H) of silver nanoclusters. The absorption peak at 1635 cm⁻¹ was attributed to C–N stretching vibrations, which was similar to the pyridine structure. The peak has been discovered in the infrared absorption spectra of the raw material ([C₄py]-[DCA]) and different purities of silver nanoclusters AgNC-[C₄py][DCA], and it has not been seen in the infrared absorption spectra of equilibrium solution outside the semipermeable membrane, so the phenomenon was explained as that 1-butylpyridine cations ([C₄py]⁺) remained in the synthesized silver nanocluster AgNC-[C₄py][DCA] system by binding to silver atoms on the Ag nanocluster surface. Instead, the series of stretching vibration absorption peaks between 2124 and 2222 cm⁻¹ were attributed to the cyano group (C≡N), which disappeared in the infrared absorption spectrum of the final product of AgNC-[C₄py][DCA] after repeated

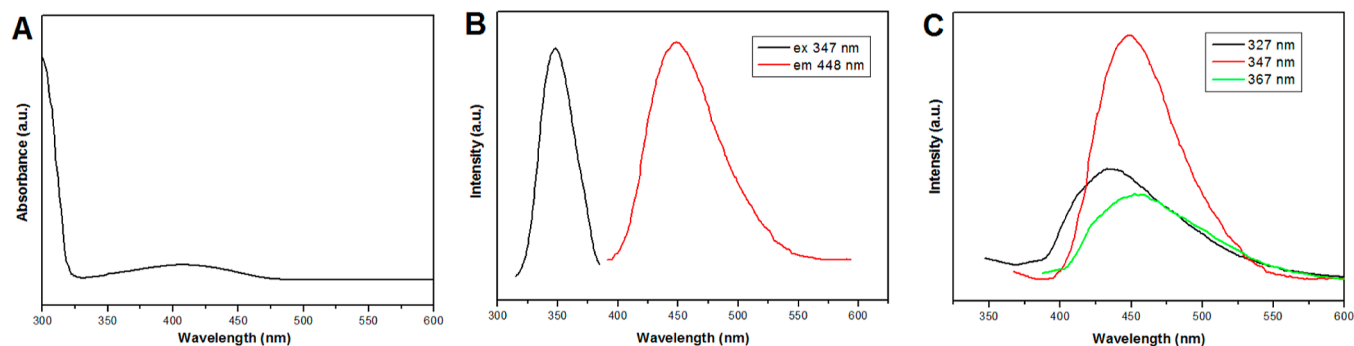


Figure 4. (A) UV-vis, (B) fluorescence excitation and emission spectra, and (C) excitation-dependent photoluminescence emission spectra of AgNC-[C₄py][DCA].

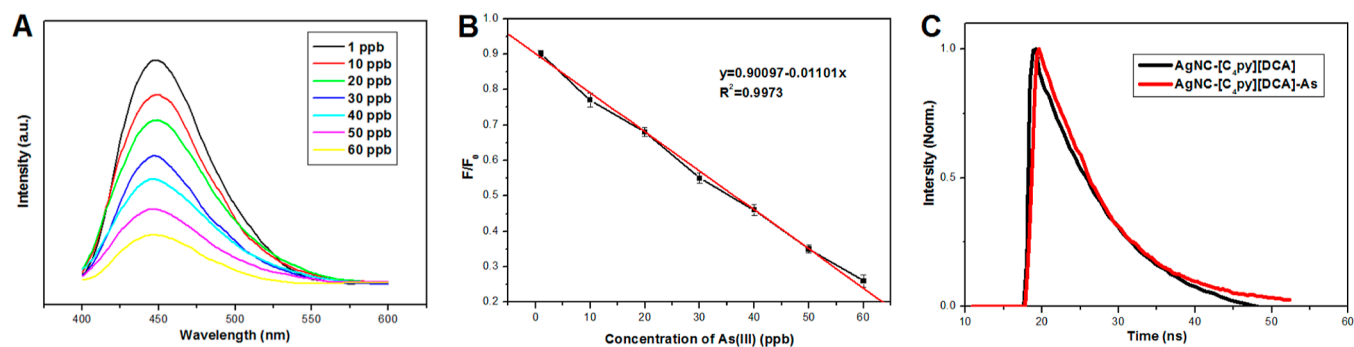


Figure 5. (A) Fluorescence emission spectra of AgNC-[C₄py][DCA] at 347 nm with different concentrations of As(III), (B) linear relationship between the fluorescence change ratio and the AsO₃³⁻ concentration, and (C) fluorescence decay curves of AgNC-[C₄py][DCA] without and with AsO₃³⁻ (the two samples were labeled AgNC-[C₄py][DCA] and AgNC-[C₄py][DCA]-As in the figure).

dialysis purification. These results indicated that the anions of dicyandiamide ([DCA]⁻) were not bonded with the silver nanoclusters, so they left the silver nanocluster AgNC-[C₄py][DCA] system through the semipermeable membrane during the purification process. The absorption peaks of the solution outside the semipermeable membrane after the initial purification were further evidence of the above process. The apparent zeta potential of AgNC-[C₄py][DCA] in Figure 3C was +48.6 mV, indicating that the silver nanoclusters were stable. In combination with the infrared spectrogram information, the positive electrical property of the silver nanocluster AgNC-[C₄py][DCA] was due to the bonding of 1-butylpyridine cations ([C₄py]⁺) to silver atoms on the surface.

The optical properties of AgNC-[C₄py][DCA] were detected by UV-vis and fluorescence spectrophotometry. As shown in Figure 4A, the absorption peak near 400 nm was classified as the surface plasmon resonance peak (SPR) of Ag nanoclusters with a small diameter,^{34–36} which was consistent with the results of DLS and TEM. In addition, the fluorescence excitation and emission spectrum of AgNC-[C₄py][DCA] (Figure 4B) showed that the maximum excitation and emission wavelengths were 347 and 448 nm, respectively, and the fluorescence emission spectrum with the best intensity of AgNC-[C₄py][DCA] can be obtained at an excitation wavelength of 347 nm (Figure 4C). At the same time, it can be seen from Figure S1 that the fluorescence performance of the silver nanocluster was very stable under different concentrations of NaCl solution and UV lamp irradiation at different times.

3.2. Detection of AsO₃³⁻. As a kind of fluorescence sensor of AsO₃³⁻ in water, AgNC-[C₄py][DCA] had excellent sensitivity and anti-interference ability. Figure 5 displays the

sensitivity of AgNC-[C₄py][DCA] to AsO₃³⁻ investigated by adding different concentrations of AsO₃³⁻ to the AgNC-[C₄py][DCA] solution. When the concentration of AsO₃³⁻ increased from 1 to 60 ppb, the fluorescence intensity of AgNC-[C₄py][DCA] decreased gradually (Figure 5A), indicating that AsO₃³⁻ gradually quenched the fluorescence of AgNC-[C₄py][DCA].

The plots with different concentrations of AsO₃³⁻ as the abscissa corresponding to the fluorescence change ratio (F/F_0) as the ordinate showed a very good linear relationship after three parallel experiments when the concentration of AsO₃³⁻ was between 1 and 60 ppb (the linear equation and linear correlation coefficient were $F/F_0 = 0.90097 - 0.01101C$ and $R^2 = 0.9973$, respectively), where the fluorescence change ratio (F/F_0) is the ratio of the fluorescence intensity of AgNC-[C₄py][DCA]-As (F) to that of original AgNC-[C₄py][DCA] (F_0 , blank). The quenching curve was well fitted with a quenching constant of $4.12 \times 10^{-2} \text{ ppb}^{-1}$ using the Stern-Volmer equation, quinine sulfate ($\Phi = 54\%$ in $0.1 \text{ mol L}^{-1} \text{ H}_2\text{SO}_4$) was chosen as the reference substance, and the fluorescence yields of AgNC-[C₄py][DCA] and AgNC-[C₄py][DCA]-As were calculated as 41 and 7%, respectively, by using the following formula.

$$\Phi_{\text{Sample}} = \Phi_{\text{Ref}} \left(\frac{n_{\text{Sample}}^2}{n_{\text{Ref}}^2} \right) \left(\frac{G_{\text{Sample}}}{G_{\text{Ref}}} \right)$$

To explore the fluorescence-quenching mechanism of AgNC-[C₄py][DCA] by AsO₃³⁻, time-correlated single-photon-counting experiments were performed to determine the fluorescence decay behavior of AgNC-[C₄py][DCA] in the absence and presence of As(III). As shown in Figure 5C, the

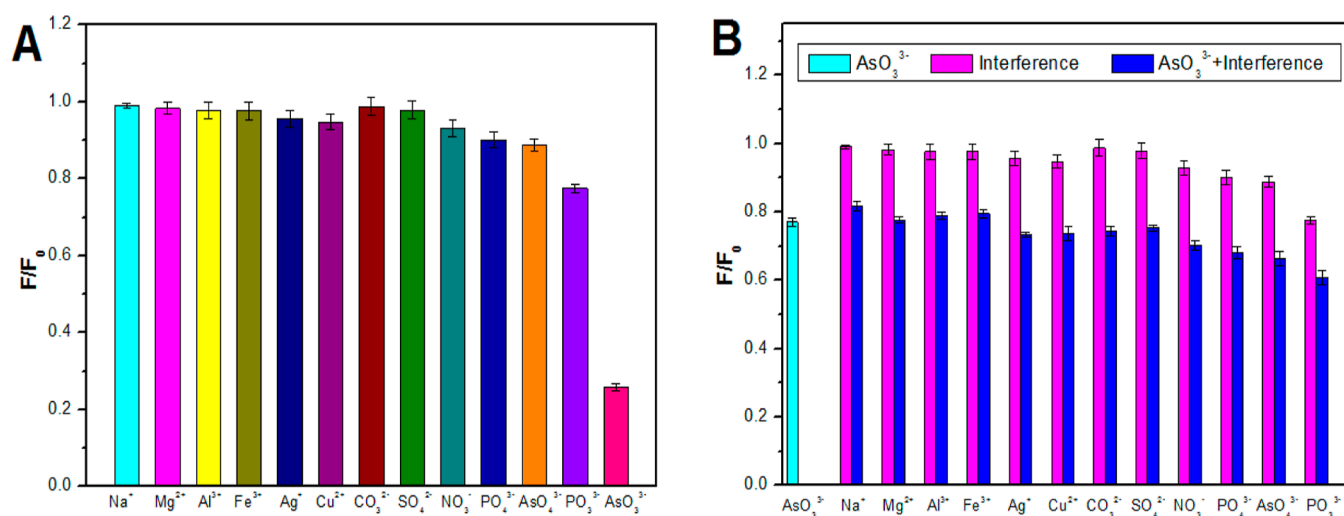


Figure 6. (A) Fluorescence change ratio F/F_0 of AgNC-[C₄py][DCA] at 347 nm on addition of different cations and anions at a concentration of 60 ppb, (B) detection result of anti-interference ability of AgNC-[C₄py][DCA] for detecting As(III). Fluorescence change ratio F/F_0 of AgNC-[C₄py][DCA] with the addition of 10 ppb AsO₃³⁻ (light blue square column), 60 ppb of different interference cations or anions (purple square column), and mixed solution of 10 ppb of AsO₃³⁻ and 60 ppb of interfering ions (dark blue square column). Note: all data in Figure 6 are statistical results of three parallel experiments.

Table 1. Performance Comparison of Different As(III) Optical Sensors

sensor	mode	linear range (ppb)	LOD (ppb)	recyclable or not	reference
Fe-GODs	fluorescence	5–100	5.10	not	23
Au@Ag NPs	SERS	0.5–10	0.1	not	25
DTT-Au NRs	colorimetry	9.7–749.9	2.80	not	38
DTT-Fe ₃ O ₄ @Au	colorimetry	0–20	0.86	not	21
CDs/TTCA-QDs	fluorescence	0–100	1	not	24
CDs/TMT-Au NPs	dual mode (fluorescence and colorimetry)	0–100/50–100	0.66/0.87	not	22
AgNC-[C ₄ py][DCA]	fluorescence	1–60	0.60	recyclable	this work

fluorescence decay of AgNC-[C₄py][DCA] without and with AsO₃³⁻ could be well fitted with the following exponential decay function to yield a life time of 7.31 and 7.03 ns, respectively. The measured fluorescence lifetimes (7.31 and 7.03 ns) did not noticeably change, suggesting a possible static quenching mechanism of AgNC-[C₄py][DCA].³⁷

$$y(t) = A_1 e^{-t/\tau_1} + A_2 e^{-t/\tau_2} + A_3 e^{-t/\tau_3}$$

$$\tau^* = \frac{A_1 \tau_1^2 + A_2 \tau_2^2 + A_3 \tau_3^2}{A_1 \tau_1 + A_2 \tau_2 + A_3 \tau_3}$$

Figures S4 and 6A display the fluorescence emission spectra and the fluorescence change ratio F/F_0 of AgNC-[C₄py][DCA] at 347 nm on addition of 60 ppb of different cations and anions, respectively, where the fluorescence change ratio is the ratio of the fluorescence intensity of the fluorescence probe after adding 60 ppb ionic solution to AgNC-[C₄py][DCA] (F) to that of original AgNC-[C₄py][DCA] (F_0 , blank). It could be clearly found that except for AsO₃³⁻, other cations (Na⁺, Mg²⁺, Al³⁺, Fe³⁺, Ag⁺, and Cu²⁺) and anions (CO₃²⁻, SO₄²⁻, NO₃⁻, PO₄³⁻, AsO₄³⁻, and PO₃³⁻) exerted a weak effect on the fluorescence performance of AgNC-[C₄py][DCA]. The above results showed that AgNC-[C₄py][DCA] is sensitive to AsO₃³⁻, and it could be used as a fluorescent sensor to detect AsO₃³⁻ efficiently.

In order to study the practicability of AgNC-[C₄py][DCA] as a fluorescence sensor for detecting AsO₃³⁻, the anti-interference ability in a complex environment was studied, and

the results are shown in Figures S5 and 6B. The interferers were 60 ppb various cations (Na⁺, Mg²⁺, Al³⁺, Fe³⁺, Ag⁺, and Cu²⁺) and anions (CO₃²⁻, SO₄²⁻, NO₃⁻, PO₄³⁻, AsO₄³⁻, and PO₃³⁻). Figures S5 and 6B display the fluorescence emission spectra and the fluorescence change ratio F/F_0 of AgNC-[C₄py][DCA] with that addition of 10 ppb AsO₃³⁻ and upon the subsequent addition of 60 ppb of different interference ions, respectively, where the fluorescence change ratio is the ratio of the fluorescence intensity of F (after adding 10 ppb AsO₃³⁻ and upon the subsequent addition of 60 ppb of interference ions) to that of F_0 (original AgNC-[C₄py][DCA], blank). As shown in Figures S5 and 6B, not only the interference ions had no obvious effect on the fluorescence performance of AgNC-[C₄py][DCA] but also the fluorescence-quenching intensity of AgNC-[C₄py][DCA] hardly changed after adding six times the concentration of interference ions to 10 ppb AsO₃³⁻. The above results indicated that the coexistence of AsO₃³⁻ and most interference ions did not affect the quantitative detection of AsO₃³⁻ by AgNC-[C₄py][DCA]. Therefore, as a kind of fluorescence sensor for quantitative detection of the AsO₃³⁻ content in water, AgNC-[C₄py][DCA] had not only high sensitivity and selectivity but also strong anti-interference ability, which is feasible in reality.

At present, many methods for the detection of As have been proposed. However, traditional arsenic detection methods have great defects because they can not effectively distinguish the highly toxic arsenic trivalent. In recent years, the development

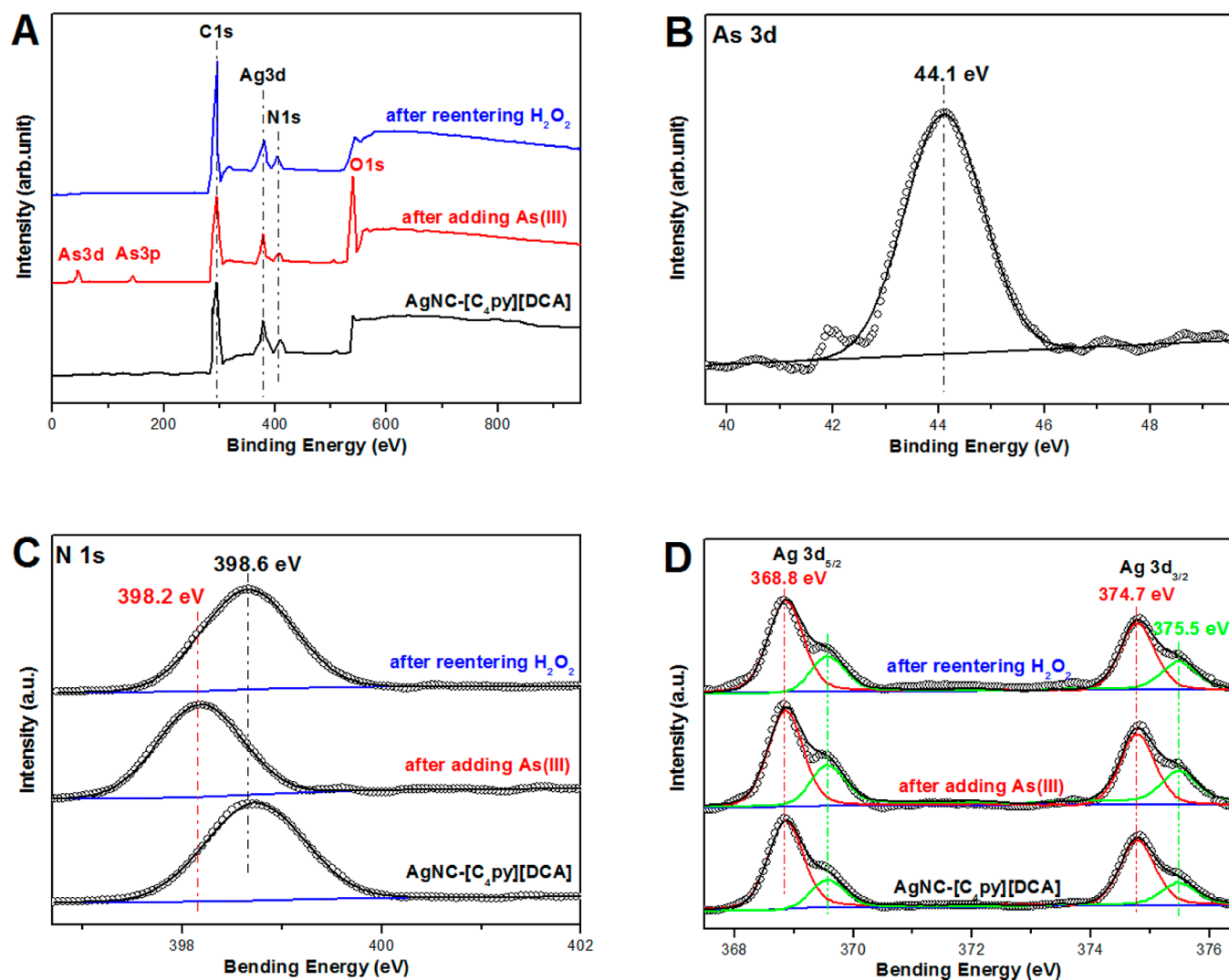


Figure 7. (A) Full scan X-ray photoelectron spectrum pattern, (C) N 1s and (D) Ag 3d high-resolution XPS patterns of the three samples with AgNC-[C₄py][DCA], after adding As(III) (the sample is labeled as AgNC-[C₄py][DCA]-As) and after re-entering H₂O₂ (the sample is labeled as AgNC-[C₄py][DCA]-As-hp), and (B) high-resolution As 3d XPS patterns of AgNC-[C₄py][DCA]-As.

of various optical sensors has realized the selective detection of As(III) to a certain extent, as shown in Table 1. AgNC-[C₄py][DCA] is one of the best metallic fluorescent materials in linear range for detecting As(III) in water. At the same time, as shown in Figure S6, AgNC-[C₄py][DCA] also is recyclable in a way other metallic nanofluorescent materials and carbon dots were not.

3.3. Possible Mechanism for the Fluorescence Response of AgNC-[C₄py][DCA] to As(III). By comparing the full scan X-ray photoelectron spectrum of solution AgNC-[C₄py][DCA], AgNC-[C₄py][DCA]-As, and AgNC-[C₄py][DCA]-As-hp (Figure 7A), we found that with the addition of As(III), two new peaks appeared near 44 and 144 eV, while these two new peaks disappeared as H₂O₂ continued to be added to the above solution. According to the handbook of X-ray photoelectron spectroscopy, these two peaks were, respectively, attributed to As 3d and 3p. Besides, as was shown in the As 3d high-resolution XPS patterns of AgNC-[C₄py][DCA]-As (Figure 7B), the binding energy of As was near 44.1 eV, which can be attributed to trivalent arsenic.³⁹ Before the full scan X-ray photoelectron spectra were detected, the three kinds of samples of AgNC-[C₄py][DCA], AgNC-

[C₄py][DCA]-As and AgNC-[C₄py][DCA]-As-hp were purified by dialysis, so As(III) was found in the AgNC-[C₄py][DCA]-As, which illustrated that the As(III) was connected to the large size of the Ag nanoclusters, instead of entering the extramembrane equilibrium solution through the semipermeable membrane, and the As element was not checked out in the sample with re-entering H₂O₂, which illustrated that As(V), made from As(III) oxidized by H₂O₂, was separated from large Ag nanoclusters and purified by a semipermeable membrane into the extramembrane equilibrium solution. The Ag 3d_{3/2} high-resolution XPS peaks of the three samples in Figure 7D can be effectively divided into two peaks with binding energies of 368.8 and 369.5 eV corresponding to free and N-bonded Ag atoms, respectively. The area ratios of the two peaks of the three samples were all near 2, which indicated that the binding mode of Ag atoms did not change significantly in the process of adding As(III) and H₂O₂ to AgNC-[C₄py][DCA] successively. Besides, as can be seen from Figure 7C, the binding energy of the N 1s high-resolution XPS peak of AgNC-[C₄py][DCA]-As (trivalent arsenic was present in the solution) was significantly smaller than that of samples AgNC-[C₄py][DCA] and AgNC-[C₄py][DCA]-As-hp

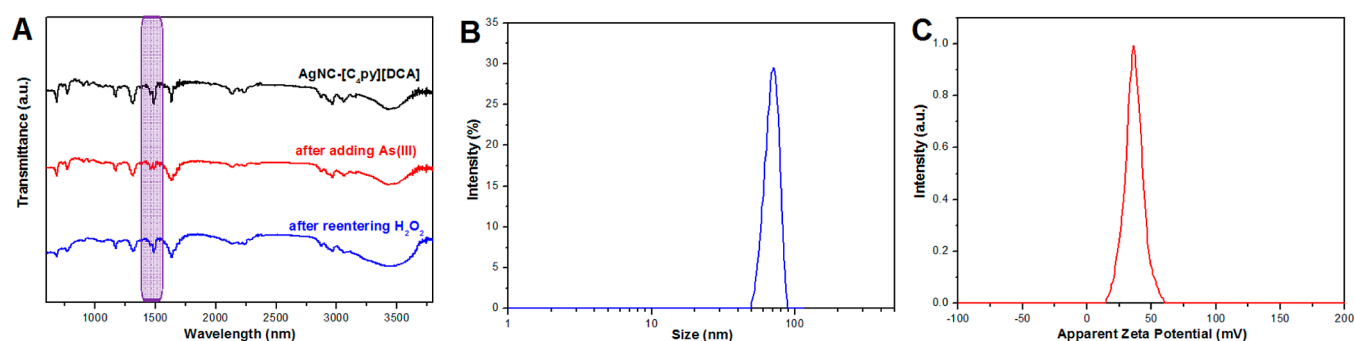


Figure 8. (A) FTIR spectra of AgNC-[C₄py][DCA], AgNC-[C₄py][DCA]-As, and AgNC-[C₄py][DCA]-As-hp, (B) DLS results, and (C) apparent zeta potential of AgNC-[C₄py][DCA]-As-hp.

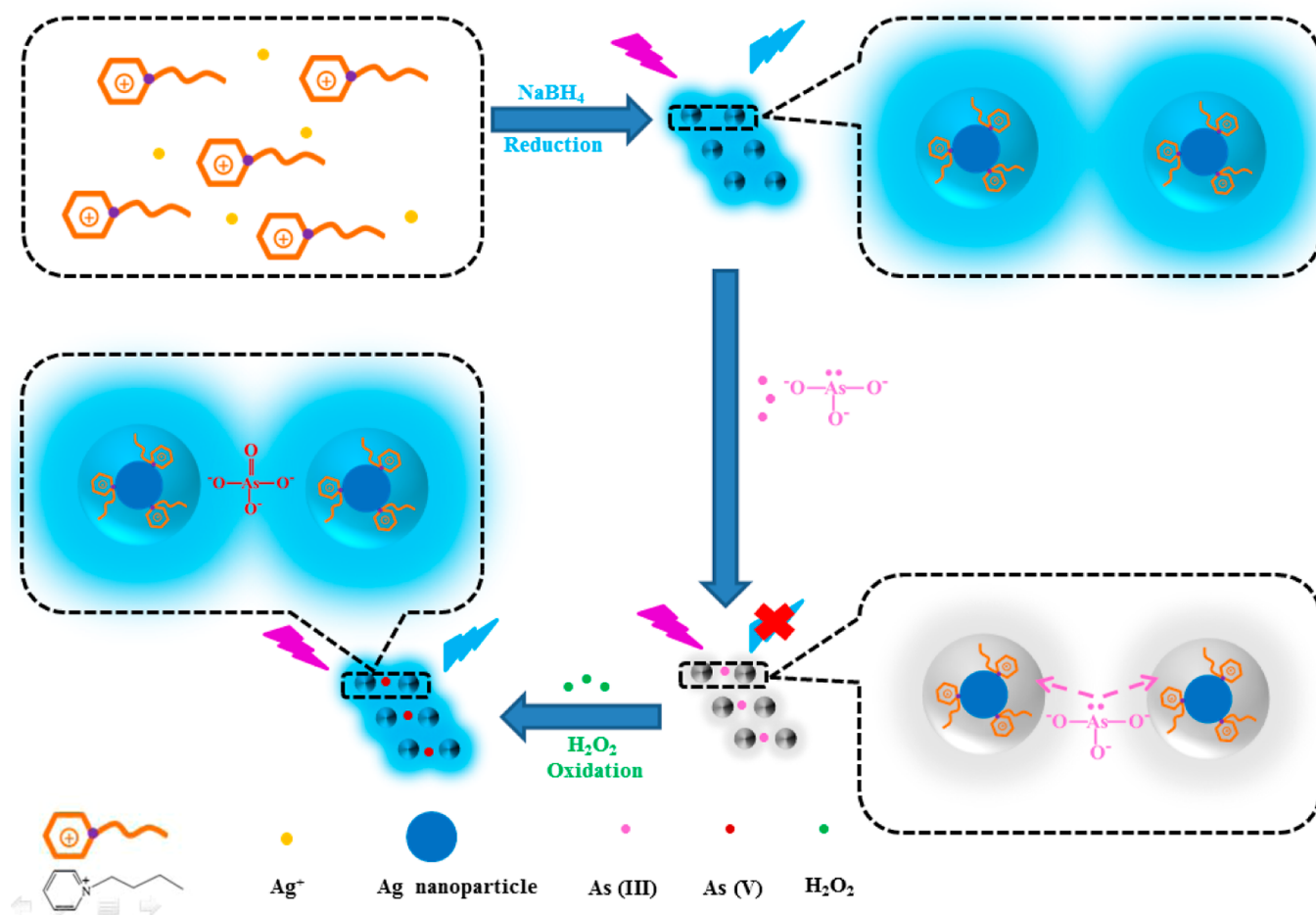


Figure 9. Working mechanism of AgNC-[C₄py][DCA] including the selective response to As(III) (fluorescence quenching) and the fluorescence recurrence after adding H₂O₂.

(trivalent arsenic was absent in either solution). Therefore, it can be concluded that As(III) was bound to large-size Ag nanoclusters by bonding with N atoms, which was the reason that it can not enter the extramembrane equilibrium solution through the semipermeable membrane during purification. As shown in Figure S2A, the apparent zeta potential of AgNC-[C₄py][DCA]-As was 0 mV, which indicated that the positive charge of the Ag nanoclusters was neutralized by the negative charge of arsenite ions.

With the addition of As(III) and H₂O₂ successively, the peak shape and half peak width of the absorption peak of pyridine structure were changed at 1635 cm⁻¹, while the absorption

peak at 1489 cm⁻¹ disappeared first and then reappeared. Combined with XPS results, the change of the infrared absorption peak near 1500 cm⁻¹ can be attributed to the interaction between As(III) and N in AgNC-[C₄py][DCA] (Figure 8A). Based on the data in Figure S6, the loss rates of fluorescence intensity of AgNC-[C₄py][DCA]-As-hp without and with semipermeable membrane purification were calculated to be 8.5% and 4.4%, respectively. Combined with the information in Figures 8B,C, S2A,B, and S3A,B, it can be seen that with the addition of As(III), the positivity of Ag nanoclusters decreased, which led to coalescence and

fluorescence quenching. After adding H₂O₂ to oxidize As(III), the above process was partially reversible.

As shown in Table S3, after three rounds of recovery and purification, the probe was used to detect 60 ppb of As(III) ions, and the spiked recoveries were calculated as 105, 111.67, and 126.67% using the equation $F/F_0 = 0.90097 - 0.01101C$. Meanwhile, in tap and river water samples, the recoveries for As(III) detection ranged from 93 to 108%, as well as the relative standard deviation was less than 3.78%, illustrating that the fluorescent probe AgNC-[C₄py][DCA] was relatively accurate for detecting As(III) in environmental water samples.

According to the fluorescence performance and structure analysis of the above materials, the working mechanism of AgNC-[C₄py][DCA] is shown in Figure 9, including the selective response to As(III) (fluorescence quenching) and the fluorescence recurrence after adding H₂O₂.

4. CONCLUSIONS

In summary, AgNC-[C₄py][DCA] was synthesized as a fluorescent probe with high selectivity and sensitivity for quantitative detection of the As(III) content in water. It showed excellent performance in terms of detection limit and linear range. What is more, the probe can be recycled with hydrogen peroxide. At the same time, the working and recovery mechanisms of the AgNC-[C₄py][DCA] probe were proposed based on the full combination of fluorescence performance, XPS spectrum, infrared spectrum, zeta potential, and other structural performance detection results, which provided a new method for the design, synthesis, and recovery of various optical probes in accordance with the idea of green chemistry.

■ ASSOCIATED CONTENT

SI Supporting Information

The Supporting Information is available free of charge at <https://pubs.acs.org/doi/10.1021/acsomega.2c02172>.

Chemical materials; fluorescence property; and apparent zeta potentials (PDF)

■ AUTHOR INFORMATION

Corresponding Author

Nannan Xing – College of Chemistry and Chemical Engineering, Huangshan University, Huangshan 245041, P. R. China; orcid.org/0000-0001-6262-7026; Email: xnnjyl@163.com

Authors

Shu Wang – College of Chemistry and Chemical Engineering, Huangshan University, Huangshan 245041, P. R. China

Enhui Zhou – College of Chemistry and Chemical Engineering, Huangshan University, Huangshan 245041, P. R. China

Xuemei Wei – College of Chemistry and Chemical Engineering, Huangshan University, Huangshan 245041, P. R. China

Ruanhui Liu – College of Chemistry and Chemical Engineering, Huangshan University, Huangshan 245041, P. R. China

Changjiang Li – College of Chemistry and Chemical Engineering, Huangshan University, Huangshan 245041, P. R. China

Le Pan – College of Chemistry and Chemical Engineering, Huangshan University, Huangshan 245041, P. R. China; orcid.org/0000-0002-1329-9078

Yuchuan Zheng – College of Chemistry and Chemical Engineering, Huangshan University, Huangshan 245041, P. R. China

Complete contact information is available at:

<https://pubs.acs.org/10.1021/acsomega.2c02172>

Notes

The authors declare no competing financial interest.

■ ACKNOWLEDGMENTS

This work was supported by the National Natural Science Foundation of China (32000992), the Natural Science Key Project of Education Department of Anhui Province (KJ2021A1039, KJ2021A1045), Undergraduate Training Programs for Innovation, Entrepreneurship of China (S202010375040, S202010089, and 202110375047), Excellent top-notch Talents Training program of Anhui Provincial Department of Education (gxyq2021214), and the Natural Science Foundation of Huangshan University (2015xkj003 and 2021JZZK007).

■ REFERENCES

- (1) Adejolu, S. B.; Khan, S.; Patti, A. F. Arsenic Contamination of Groundwater and its Implications for Drinking Water Quality and Human Health in Under-developed Countries and Remote Communities—a Review. *Appl. Sci.* **2021**, *11*, 1926.
- (2) Nordstrom, D. K. Worldwide Occurrences of Arsenic in Ground Water. *Science* **2002**, *296*, 2143–2145.
- (3) Xie, J.; Schofield, J. R. M.; Liao, L.; Peng, H.; Uppal, J. S.; Zheng, Q.; Le, X. C. Simultaneous Removal of Arsenic and Antimony from Mining Wastewater. *J. Environ. Sci.* **2020**, *93*, 117–119.
- (4) Guo, Q.; He, T.; Wu, Q.; Liu, M. Constraints of Major Ions and Arsenic on the Geological Genesis of Geothermal Water: Insight from a Comparison between Xiong'an and Yangbajain, two Hydrothermal Systems in China. *Appl. Geochem.* **2020**, *117*, 104589.
- (5) Vandana, U. K.; Gulzar, A. B. M.; Singha, L. P.; Bhattacharjee, A.; Mazumder, P. B.; Pandey, P. Hyperaccumulation of Arsenic by *Pteris Vittata*, a Potential Strategy for Phytoremediation of Arsenic-contaminated Soil. *Environ. Sustainability* **2020**, *3*, 169–178.
- (6) Alsen, M.; Sinclair, C.; Cooke, P.; Ziadkhanpour, K.; Genden, E.; van Gerwen, M. Endocrine Disrupting Chemicals and Thyroid Cancer: An Overview. *Toxics* **2021**, *9*, 14.
- (7) Kolya, H.; Kuila, T.; Kim, N. H.; Lee, J. H. Colorimetric/Naked Eye Detection of Arsenic Ions in Aqueous Medium by Mango Flower Extract: A Facile and Novel Approach. *Appl. Surf. Sci.* **2020**, *513*, 145760.
- (8) Zong, C.; Jin, X.; Liu, J. Critical Review of Bio/nano Sensors for Arsenic Detection. *Trends Environ. Anal. Chem.* **2021**, *32*, No. e00143.
- (9) Reid, M. S.; Hoy, K. S.; Schofield, J. R. M.; Uppal, J. S.; Lin, Y.; Lu, X.; Peng, H.; Le, X. C. Arsenic Speciation Analysis: A Review with an Emphasis on Chromatographic Separations. *TrAC, Trends Anal. Chem.* **2020**, *123*, 115770.
- (10) Huo, J.-B.; Yu, G. Mesoporous Cerium Oxide-anchored Magnetic Polyhedrons Derived from MIL-100(Fe) for Enhanced Removal of Arsenite from Aqueous Solution. *J. Hazard. Mater.* **2021**, *415*, 125709.
- (11) Xiao, J.; Zhang, S.; Tu, B.; Jiang, X.; Cheng, S.; Tang, Q.; Zhang, J.; Qin, X.; Wang, B.; Zou, Z.; Chen, C. Arsenite Induces Ferroptosis in the Neuronal Cells via Activation of Ferritinophagy. *Food Chem. Toxicol.* **2021**, *151*, 112114.
- (12) Syam Babu, D.; Nidheesh, P. V.; Suresh Kumar, M. Arsenite Removal from Aqueous Solution by Aerated Iron Electrocoagulation process. *Sep. Sci. Technol.* **2021**, *56*, 184–193.

- (13) Stratton, G.; Whitehead, H. C. Colorimetric Determination of Arsenic in Water with Silver Diethyldithiocarbamate. *J.—Am. Water Works Assoc.* **1962**, *54*, 861–864.
- (14) Kundu, S.; Ghosh, S.; Mandal, M.; Pal, T.; Pal, A. Spectrophotometric Determination of Arsenic via Arsine Generation and In-situ Colour Bleaching of Methylene blue (MB) in Micellar Medium. *Talanta* **2002**, *58*, 935–942.
- (15) Hsieh, C.-J.; Yen, C.-H.; Kuo, M.-S. Determination of Trace Amounts of Arsenic (III) and Arsenic (V) in Drinking Water and Arsenic (III) Vapor in Air by Graphite-furnace Atomic Absorption Spectrophotometry Using 2,3-dimercaptopropane-1-sulfonate as a Complexing Agent. *Anal. Sci.* **1999**, *15*, 669–673.
- (16) B'Hymer, C.; Caruso, J. A. Arsenic and its Speciation Analysis Using High-performance Liquid Chromatography and Inductively Coupled Plasma Mass Spectrometry. *J. Chromatogr. A* **2004**, *1045*, 1–13.
- (17) Al-assaf, K. H.; Tyson, J. F.; Uden, P. C. Determination of Four Arsenic Species in Soil by Sequential Extraction and High Performance Liquid Chromatography with Post-column Hydride Generation and Inductively Coupled Plasma Optical Emission Spectrometry Detection. *J. Anal. At. Spectrom.* **2009**, *24*, 376–384.
- (18) Lai, G.; Chen, G.; Chen, T. Speciation of As^{III} and As^V in Fruit Juices by Dispersive Liquid–liquid Microextraction and Hydride Generation-atomic Fluorescence Spectrometry. *Food Chem.* **2016**, *190*, 158–163.
- (19) Luo, H.; Wang, X.; Dai, R.; Liu, Y.; Jiang, X.; Xiong, X.; Huang, K. Simultaneous Determination of Arsenic and Cadmium by Hydride Generation Atomic Fluorescence Spectrometry Using Magnetic Zero-valent Iron Nanoparticles for Separation and Pre-concentration. *Microchem. J.* **2017**, *133*, 518–523.
- (20) Boruah, B. S.; Daimari, N. K.; Biswas, R. Functionalized Silver Nanoparticles as an Effective Medium towards Trace Determination of Arsenic (III) in Aqueous Solution. *Results Phys.* **2019**, *12*, 2061–2065.
- (21) Banerjee, S.; Kumar, N. P.; Srinivas, A.; Roy, S. Core-Shell Fe₃O₄@Au Nanocomposite as Dual-Functional Optical Probe and Potential Removal System for Arsenic(III) from Water. *J. Hazard. Mater.* **2019**, *375*, 216–223.
- (22) Li, J.; Yang, L.; Ruan, Y.; Chu, S.; Wang, H.; Li, Z.; Jiang, C.; Liu, B.; Yang, L.; Zhang, Z. Dual-mode Optical Nanosensor Based on Gold Nanoparticles and Carbon Dots for Visible Detection of As (III) in Water. *ACS Appl. Nano. Mater.* **2020**, *3*, 8224–8231.
- (23) Pathan, S.; Jalal, M.; Prasad, S.; Bose, S. Aggregation-induced Enhanced Photoluminescence in Magnetic Graphene Oxide Quantum Dots as a Fluorescence Probe for As(III) Sensing. *J. Mater. Chem. A* **2019**, *7*, 8510–8520.
- (24) Sun, Q.; Yang, L.; Su, L.; Liu, W.; Wang, Y.; Yu, S.; Jiang, C.; Zhang, Z. Colloidal Quantum Dot Chains: Self-Assembly Mechanism and Ratiometric Fluorescent Sensing. *RSC Adv.* **2017**, *7*, 53977–53983.
- (25) Song, L.; Mao, K.; Zhou, X.; Hu, J. A Novel Biosensor Based on Au@Ag Core-Shell Nanoparticles for SERS Detection of Arsenic(III). *Talanta* **2016**, *146*, 285–290.
- (26) Nallepalli, P.; Tomé, L. C.; Vijayakrishna, K.; Marrucho, I. M. Imidazolium-Based Copoly (Ionic Liquid) Membranes for CO₂/N₂ Separation. *Ind. Eng. Chem. Res.* **2019**, *58*, 2017–2026.
- (27) Bai, L.; Wang, T.; Weisensee, P. B.; Liu, X.; He, M. Two-Binary-Interaction-Parameter Model for Molecular Solute + Ionic Liquid Solution. *Ind. Eng. Chem. Res.* **2021**, *60*, 11490–11501.
- (28) Fan, B.; Wei, J.; Ma, X.; Bu, X.; Xing, N.; Pan, Y.; Zheng, L.; Guan, W. Synthesis of Lanthanide-Based Room Temperature Ionic Liquids with Strong Luminescence and Selective Sensing of Fe(III) over Mixed Metal Ions. *Ind. Eng. Chem. Res.* **2016**, *55*, 2267–2271.
- (29) Ma, X.-X.; Wei, J.; Guan, W.; Pan, Y.; Zheng, L.; Wu, Y.; Yang, J.-Z. Ionic Parachor and its Application to Pyridinium-Based Ionic Liquids of {[C_npy][DCA]} (n = 2, 3, 4, 5,6). *J. Chem. Thermodyn.* **2015**, *89*, 51–59.
- (30) Xing, N.; Liang, K.; Fang, D.; Guan, W.; Yang, J. The Molar Surface Gibbs Energy and its Application to the Binary Mixtures of N-Butylpyridinium Dicyanamide [C₄py][DCA] with Alcohols. *J. Chem. Thermodyn.* **2019**, *128*, 283–294.
- (31) Xing, N.; Dai, B.; Ma, X.; Wei, J.; Pan, Y.; Guan, W. The Molar Surface Gibbs Energy and Prediction of Surface Tension of [C_npy][DCA] (n = 3,4,5). *J. Chem. Thermodyn.* **2016**, *95*, 21–25.
- (32) Li, J.; Qiao, Y.; Ding, Z.; Liu, X. Microstructure and Properties of Ag/N Dual Ions Implanted Titanium. *Surf. Coat. Technol.* **2011**, *205*, 5430–5436.
- (33) Alhokbany, N.; Ahama, T.; Ruksana; Naushad, M.; Alshehri, S. M. AgNPs Embedded N-doped Highly Porous Carbon Derived from Chitosan Based Hydrogel as Catalysts for the Reduction of 4-Nitrophenol. *Composites, Part B* **2019**, *173*, 106950.
- (34) Chen, J.; Cheng, Y.; Li, H.; Fang, C.; Li, H.; Wang, K. Synthesis of Stable Ag NPs Solution via Anionic Polyacrylamide Template Method as Sensitive Fluorescence Sensor for Detecting Heavy Metal Ions. *Chem. Lett.* **2019**, *48*, 1448–1451.
- (35) Petty, J. T.; Zheng, J.; Hud, N. V.; Dickson, R. M. DNA-Templated Ag Nanocluster Formation. *J. Am. Chem. Soc.* **2004**, *126*, 5207–5212.
- (36) Xiao, Y.; Zhang, Y.; Huang, H.; Zhang, Y.; Du, B.; Chen, F.; Zheng, Q.; He, X.; Wang, K. Conjugated Polyelectrolyte-Stabilized Silver Nanoparticles Coupled with Pyrene Derivative for Ultra-sensitive Fluorescent Detection of Iodide. *Talanta* **2015**, *131*, 678–683.
- (37) Shellaiah, M.; Awasthi, K.; Chandran, S.; Azaad, B.; Sun, K. W.; Ohta, N.; Wu, S.-P.; Lin, M.-C. Methylammonium Tin Tribromide Quantum Dots for Heavy Metal Ion Detection and Cellular Imaging. *ACS Appl. Nano Mater.* **2022**, *5*, 2859–2874.
- (38) Chandra, V.; Park, J.; Chun, Y.; Lee, J. W.; Hwang, I.-C.; Kim, K. S. Water-Dispersible Magnetite-Reduced Graphene Oxide Composites for Arsenic Removal. *ACS Nano* **2010**, *4*, 3979–3986.
- (39) Zhang, T.; Zhao, Y.; Bai, H.; Liu, Y.; Liu, Y.; Zhang, Q. Efficient As (III) Removal Directly as Basic Iron Arsenite by In-Situ Generated Fe (III) Hydroxide from Ferrous Sulfate on the Surface of CaCO₃. *Appl. Surf. Sci.* **2019**, *493*, 569–576.